nature neuroscience

Inactivity-induced increase in nAChRs upregulates Shal K^+ channels to stabilize synaptic potentials

Yong Ping & Susan Tsunoda

Long-term synaptic changes, which are essential for learning and memory, are dependent on homeostatic mechanisms that stabilize neural activity. Homeostatic responses have also been implicated in pathological conditions, including nicotine addiction. Although multiple homeostatic pathways have been described, little is known about how compensatory responses are tuned to prevent them from overshooting their optimal range of activity. We found that prolonged inhibition of nicotinic acetylcholine receptors (nAChRs), the major excitatory receptors in the *Drosophila* CNS, resulted in a homeostatic increase in the *Drosophila* α7 (Dα7)-nAChR. This response then induced an increase in the transient A-type K^+ current carried by Shaker cognate L (Shal; also known as voltage-gated K^+ channel 4, Kv4) channels. Although increasing Dα7-nAChRs boosted miniature excitatory postsynaptic currents, the ensuing increase in Shal channels served to stabilize postsynaptic potentials. These data identify a previously unknown mechanism for fine tuning the homeostatic response.

Maintaining neural activity within an optimal range while allowing for the storage of long-term changes in synaptic strength is an important challenge for the nervous system[1]. Homeostatic synaptic plasticity has widely been received as a mechanism by which neuronal circuits preserve stability when presented with changes in activity. Synaptic inactivity has been shown to result in an increase in the number of postsynaptic GluA1- or GluA2-containing receptors and/or release of presynaptic vesicles in mammalian neurons, as well as at the neuromuscular junction (NMJ)[1–3]. Although multiple homeostatic feedback mechanisms exist for scaling up synaptic strength, maintaining activity within an optimal range must also require precise tuning of activity to prevent over-shooting the target range. Downstream control mechanisms are likely to exist, although no examples have been reported.

Most cell-intrinsic responses to activity blockade have been reported to contribute to the homeostatic response[4–6]. For example, in cultured cortical pyramidal neurons, activity blockade results in an increased voltage-dependent Na^+ current and a reduced delayed rectifier-type K^+ current, both of which are predicted to increase excitability[4]. By contrast, deprivation of visual input during the critical period of development reduces the intrinsic excitability of pyramidal neurons in the visual cortex[7]. In all cases, little is known about the signaling pathways that induce these intrinsic changes, how these changes are regulated and their roles in synaptic homeostasis[1].

Homeostasis has also been suggested to underlie the upregulation of neuronal nAChRs following prolonged exposure to nicotine[8]. Although nicotine is an agonist, extended exposure to low levels of nicotine leads to nAChR desensitization, which is thought to trigger homeostatic pathways[9,10]. The increased number of nAChRs is thought to contribute to both the increased sensitivity to nicotine when receptors are available for activation and, conversely, tolerance to nicotine when receptors are desensitized[8,9]. A greater understanding of the homeostatic regulation of nAChRs is likely to provide insight into the pathogenesis of nicotine addiction.

In this study, we blocked nAChRs, which mediate the vast majority of fast excitatory synaptic transmission in central *Drosophila* neurons, and revealed a homeostatic increase in the miniature excitatory postsynaptic current (mEPSC) carried by newly translated Dα7-nAChRs (encoded by *nAcRα-18C*). We showed that this increase in Dα7-nAChR induced an increase in expression and function of the transient A-type Shal K^+ channel, and that this increase was triggered by greater Ca^{2+} influx through Dα7 receptors and subsequent calmodulin kinase II (CaMKII) activation. Although increasing Dα7-nAChR boosted mEPSCs, the ensuing increase in Shal K^+ channels evoked a previously unknown mechanism to stabilize synaptic potentials.

RESULTS

Homeostatic increase in mEPSCs in excitatory neurons

To examine homeostatic changes at interneuronal synapses in *Drosophila*, we began by using primary cultures from late-gastrula-stage embryos. These cultures have been well studied with respect to voltage-dependent currents and synaptic physiology[11–14], allow the labeling of identified neurons for analysis[15,16], and have been shown to exhibit stable, matured electrical properties after 3 days[13]. As nAChRs mediate the vast majority of fast excitatory synaptic events in the *Drosophila* CNS[13,16], we blocked synaptic activity with curare, which completely eliminates mEPSCs (**Supplementary Fig. 1a**). To analyze identified neurons, specific *GAL4* lines were used to drive expression of *UAS*-controlled mouse CD8-EGFP (*UAS–mCD8-EGFP*): *RRa-GAL4* or *RN2-GAL4* lines were used to drive expression in anterior corner cell and 'raw prawn' 2 motor neurons, respectively, *GH146-GAL4* was used to drive expression in projection neurons (which receive input from olfactory neurons and project to higher centers in the brain) and *EL-GAL4* was used to drive expression in the lateral cluster of even-skipped-expressing cells (which are reported to be exclusively interneurons)[17].

Department of Biomedical Sciences, Colorado State University, Fort Collins, Colorado, USA. Correspondence should be addressed to S.T. (susan.tsunoda@colostate.edu).

Received 14 July; accepted 9 September; published online 13 November 2011; doi:10.1038/nn.2969

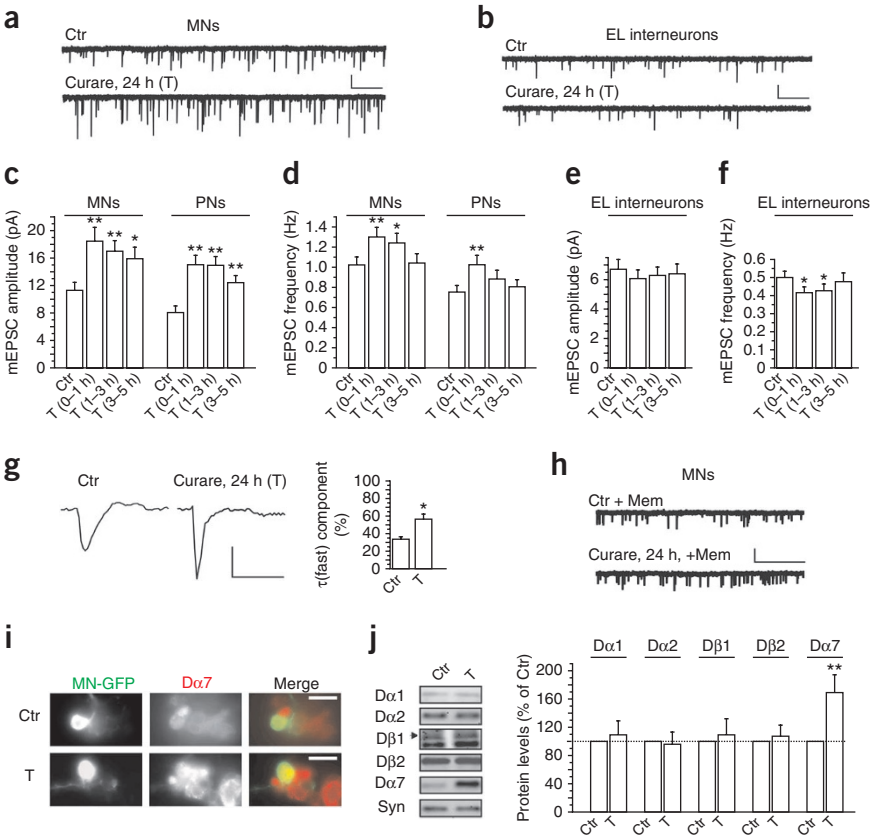

Figure 1 Synaptic blockade induced an increase in Dα7 receptors. (**a**,**b**) mEPSCs from motor neurons (MNs, **a**) and lateral cluster even-skipped-expressing (EL) interneurons (**b**) in cultures that were mock treated (Ctr) or curare treated (T). Scale bars: 10 pA, 5 s. (**c**,**d**) mEPSC amplitude (**c**) and frequency (**d**) from control and treated cultures. $n = 9$–15. PN, projection neuron. (**e**,**f**) mEPSC amplitude (**e**) and frequency (**f**) from control and treated cultures from lateral cluster even-skipped-expressing interneurons. $n = 7$–11. (**g**) mEPSCs from control and treated cells (left). Deactivation of mEPSCs fit with a double exponential function: relative amplitudes of the τ(fast) component are shown $n = 12$ (control) and 27 (treated). Scale bars: 10 pA, 5 ms. See also **Supplementary Figure 2**. (**h**) mEPSCs recorded from motor neurons with 30 μM memantine (Mem) from control and treated cultures. Mean (± s.e.m.) amplitudes showed no significant difference between control and treated cells. $n = 12$ (control) and 10 (treated). Scale bars: 10 pA, 5 s. (**i**) Control and treated cultures immunostained for the Dα7 receptor (red). Each cluster includes a single GFP-labeled motor neuron. Scale bars: 10 μm. (**j**) Immunoblots (left) and quantification (right) of steady-state levels of Dα1, Dα2, Dβ1 (arrowhead), Dβ2 and Dα7 from control and treated brains. Protein levels were normalized to Syntaxin (Syn) ($n = 4$). Error bars: s.e.m. $^*P < 0.05$, $^{**}P < 0.01$, Student's t test. See also **Supplementary Figure 3** and **Supplementary Table 1**. Full-length blots and gels are shown in **Supplementary Figure 9**.

We blocked synaptic activity with curare in the culture medium, then washed out the antagonist for ~3 min and allowed the cultures to recover for 30 min in fresh medium. Medium was then changed to extracellular recording solution, and mEPSCs were recorded from EGFP-labeled neurons. This treatment protocol is referred to as protocol 1 (see Online Methods). When synaptic activity was blocked for up to 12 h, no changes in mEPSCs were observed (**Supplementary Fig. 1c**–**f**). With 24 h of synaptic inhibition, however, there was a clear increase in mEPSC amplitude and frequency in the excitatory motor neurons (control neurons, 11.3 ± 1.1 pA; treated neurons, 18.5 ± 2.0 pA) and projection neurons (control, 8.0 ± 0.9 pA; treated, 15.1 ± 1.2 pA) (**Fig. 1** and **Supplementary Fig. 1g**). By contrast, lateral cluster even-skipped-expressing interneurons showed a slight decrease in mEPSC frequency, and only immediately after washout of antagonist (**Fig. 1b**,**e**,**f** and **Supplementary Fig. 1h**). Enhancement of mEPSCs in excitatory neurons was long-lasting, persisting for hours after antagonist washout (**Fig. 1c**,**d**). As no substantial difference in dendritic branching, quantified at radial intervals from the soma of single neurons, were observed between treated and control neurons (**Supplementary Fig. 1i**), changes in mEPSCs are not likely to be due to major structural changes induced by curare treatment. Increases in mEPSC amplitude and frequency in motor neurons and projection neurons in response to activity blockade were similar to the homeostatic responses reported for glutamatergic mammalian neurons. Thus, although it is mediated by different receptors, excitatory synaptic homeostasis seems to be a conserved phenomenon betweeen *Drosophila* and mammalian central neurons.

Inactivity-induced upregulation of Dα7-nAChR

An increase in mEPSC amplitude suggests that there has been an enhancement in the function or number of postsynaptic nAChRs. Notably, mEPSCs recorded from curare-treated motor neurons also had a faster rate of decay than mEPSCs of untreated motor neurons (**Fig. 1g**). When mEPSC decays were fit with a double exponential function, we found a similar fast component (τ(fast)) in both mock- and curare-treated motor neurons (control, 0.32 ± 0.03 ms; treated, 0.27 ± 0.03 ms). However, the contribution of this τ(fast) was significantly increased with synaptic blockade ($P < 0.05$; **Fig. 1g**). This result suggested that the increased mEPSC amplitudes were due to upregulation of a particular subtype of nAChR. Notably, vertebrate α7-nAChRs have been shown to have faster deactivation kinetics than other subtypes[18,19]. Although there is a paucity of specific inhibitors for these vertebrate receptors, memantine has previously been used to block them[20]. Indeed, we found that the increase in mEPSC amplitude following curare treatment was blocked when memantine was used during recording (control, 8.3 ± 0.9 pA; treated, 8.7 ± 0.9 pA) (**Fig. 1h**), suggesting that the increase is memantine sensitive and therefore probably carried by Dα7 receptors. To examine whether the increase in mEPSC amplitude was due to an increase in Dα7 receptor number, we used an antibody to Dα7 (anti-Dα7) to immunostain cultures that were either mock or curare treated for 24 h. Indeed, we observed a clear and reproducible increase in Dα7 signal in most neurons, including GFP-labeled motor neurons, from curare-treated cultures compared with the signal from mock-treated cultures (**Fig. 1i**).

We next examined whether the increase in Dα7 induced by synaptic blockade could be observed in adult brains *in vivo* and, further, whether this homeostatic response was specific to the Dα7 subunit. To do this, whole brains were mock or curare treated in culture; cell viability was confirmed by showing that protein synthesis could indeed be induced in cultured brains (**Supplementary Fig. 1j**). We incubated wild-type brains in culture medium either with or without curare for 15 min, 12 h or 24 h, and protein levels were analyzed by immunoblot analysis. Notably, we found that Dα7 protein levels were increased by more

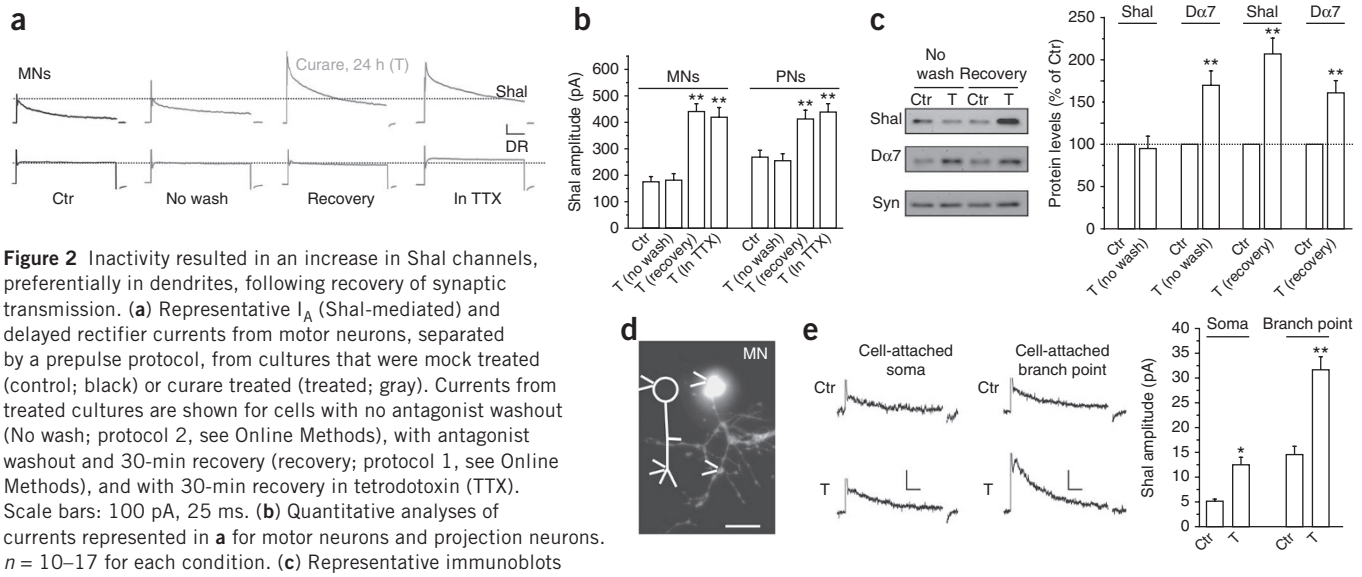

Figure 2 Inactivity resulted in an increase in Shal channels, preferentially in dendrites, following recovery of synaptic transmission. (**a**) Representative I_A (Shal-mediated) and delayed rectifier currents from motor neurons, separated by a prepulse protocol, from cultures that were mock treated (control; black) or curare treated (treated; gray). Currents from treated cultures are shown for cells with no antagonist washout (No wash; protocol 2, see Online Methods), with antagonist washout and 30-min recovery (recovery; protocol 1, see Online Methods), and with 30-min recovery in tetrodotoxin (TTX). Scale bars: 100 pA, 25 ms. (**b**) Quantitative analyses of currents represented in **a** for motor neurons and projection neurons. $n = 10–17$ for each condition. (**c**) Representative immunoblots (left; three brains per lane) and quantitative analyses (right) for steady-state levels of Shal and Dα7 from control cells, and from whole-brain treated cultures without antagonist washout (no wash) and with a 1-h washout (recovery). $n = 4$. (**d**,**e**) Cell-attached recordings from representative GFP-labeled motor neurons at the soma and at the branch point on a dendrite (~30 μm from the soma), as indicated (**e**). Shown are representative Shal currents isolated by a prepulse protocol, and quantitative analyses of Shal amplitudes before and after curare treatment. Scale bars: 10 μm (**d**), and 10 pA, 20 ms (**e**). Error bars: s.e.m. $*P < 0.05$ and $**P < 0.01$, Student's *t* test. See also **Supplementary Figure 2**. Full-length blots and gels are shown in **Supplementary Figure 9**.

than 60% after 24 h of curare treatment (**Fig. 1j**), but no differences were observed with shorter incubations. In addition, similarly to the enhancement in mEPSCs, the increase in Dα7 protein persisted for at least 5 h (**Supplementary Fig. 1b**). By contrast, other nAChR subunits, including Dα1, Dα2, Dβ1 and Dβ2, showed no significant change following synaptic inactivity (**Fig. 1j**). Altogether, our results showed a selective increase in Dα7 receptors that probably underlay the increased amplitudes of mEPSCs following prolonged synaptic block.

Inactivity-induced increase in Shal K^+ currents

Homeostasis can be achieved by synaptic and/or cell-intrinsic changes. Indeed, other systems have demonstrated cell-intrinsic changes after activity blockade[4–7,21]. However, how these intrinsic changes are triggered by synaptic inactivity has remained a mystery. We set out to investigate whether cell-intrinsic changes also occur in our system, and planned to examine how these changes are triggered by synaptic blockade. As all of the voltage–dependent K^+ channels and currents have been genetically and electrophysiologically identified in the cultured neurons we used[11,12], we first examined whether I_A currents carried by Shal channels or delayed rectifier currents carried by Shab (also known as Kv2) and Shaw (also known as Kv3) channels were changed in response to curare treatment. We blocked synaptic activity with curare using treatment protocol 1, as performed for mEPSC recordings (see Online Methods), and conducted voltage procedures to isolate delayed rectifier and I_A currents. We found that I_A currents carried by Shal K^+ channels were markedly increased in motor neurons (from 176 ± 22 pA to 438 ± 30 pA) and projection neurons (from 269 ± 26 pA to 413 ± 35 pA) (**Fig. 2a**,**b**), with no change in cell size, as indicated by capacitance measurements (**Supplementary Table 1**). No changes in I_A and delayed rectifier currents were observed in lateral cluster even-skipped-expressing interneurons (**Supplementary Fig. 3d**). Notably, however, when antagonist was not washed out (protocol 2; see Online Methods), no changes in I_A or delayed rectifier currents were observed in either motor neurons or projection neurons (**Fig. 2a**,**b**). These results suggest that prolonged synaptic inhibition resulted in a selective increase in Shal K^+ current density in excitatory neurons. Upregulation of Shal required recovery of synaptic transmission, but was independent of action potential firing, as it occurred even in the presence of tetrodotoxin (**Fig. 2a**,**b**).

To test whether the increase in I_A was due to an increase in the number of Shal K^+ channels, we examined whole brains following curare treatment. Levels of Shal protein from brains examined immediately after mock or curare treatment (protocol 2) were not significantly different ($P > 0.05$; **Fig. 2c**). However, when synaptic transmission was allowed to recover for 60 min (protocol 1), there was an ~80% increase in Shal protein (**Fig. 2c**). As was the case for Dα7, this increase in Shal was seen only after 24 h of curare treatment and persisted for at least 5 h (**Supplementary Fig. 3a**). Altogether, our results showed that prolonged blockade of synaptic activity resulted in an increase in the number of Shal K^+ channels and that this increase required recovery of synaptic activity. By contrast, treatment protocols 1 (wash and recovery) and 2 (no wash) both resulted in an up–regulation of Dα7, suggesting that the increase in Dα7 did not require recovery of synaptic activity following blockade (**Fig. 2c**).

As Shal K^+ currents are important for neuronal firing[15], we speculated that the upregulation of Shal channels should also affect the firing behavior of cells. We curare-treated wild-type cultures for 24 h, washed out antagonist with medium and then monitored firing during the following 30 min (treatment protocol 3, see Online Methods), when Shal channels should be actively upregulated. We compared motor neuron firing patterns at 5–10 min and then at 25–30 min after a 500 ms current injection of 60 pA. We found that the number of action potentials fired decreased during this recovery period (**Supplementary Fig. 4**). Shal channels have been shown to affect both latency to action potential firing and firing frequency in these neurons[15,22], so these changes are consistent with an increase in Shal channels during this recovery period following synaptic blockade.

To gain insight into whether Shal channels were preferentially upregulated in a particular subcellular region of neurons, we recorded Shal channel activity in cell-attached patches from the somas and dendrites

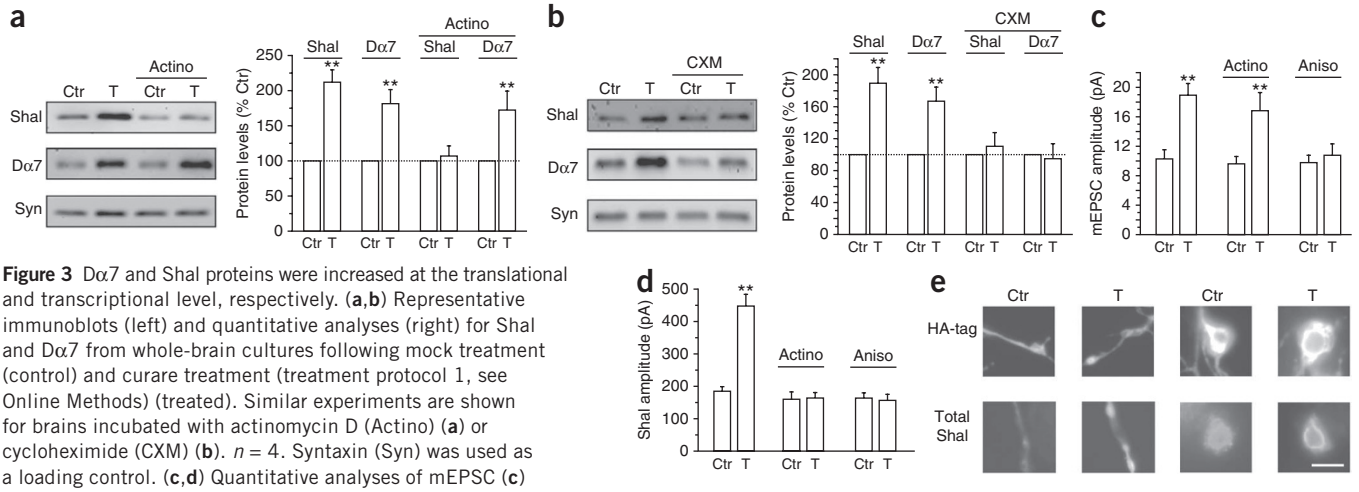

Figure 3 Dα7 and Shal proteins were increased at the translational and transcriptional level, respectively. (**a**,**b**) Representative immunoblots (left) and quantitative analyses (right) for Shal and Dα7 from whole-brain cultures following mock treatment (control) and curare treatment (treatment protocol 1, see Online Methods) (treated). Similar experiments are shown for brains incubated with actinomycin D (Actino) (**a**) or cycloheximide (CXM) (**b**). $n = 4$. Syntaxin (Syn) was used as a loading control. (**c**,**d**) Quantitative analyses of mEPSC (**c**) and I_A (Shal-mediated) (**d**) amplitudes from motor neurons following mock and curare treatment; cultures were incubated with actinomysin D or anisomycin (Aniso) throughout treatment protocol 1 (see Online Methods). $n = 9$–14 for each condition. (**e**) Representative immunostaining for HA and Shal in motor neuron dendrites (~50 μm from the soma) and somas from a transgenic line expressing HA-Shal. Note that after a 24-h curare treatment (treated), there was an increase in total Shal signal but no change in HA signal in both dendrites and somas. Error bars: s.e.m. $^{**}P < 0.01$, Student's *t* test. Full-length blots and gels are shown in **Supplementary Figure 10**, quantification of immunostaining is shown in **Supplementary Figure 5b**, and recorded Shal currents from control and treated HA-Shal-expressing motor neurons are shown in **Supplementary Figure 5c.** Scale bar: 10 μm.

of motor neurons. We compared Shal currents in patches from cells that were mock or curare treated according to protocol 1 (wash and recovery; see Online Methods) to induce the upregulation of Shal. Cell-attached patches from dendrites were obtained from a branch point ~30 μm from the soma (**Fig. 2d**). We found that Shal currents were increased following curare treatment in patches from both the cell body and dendrites (**Fig. 2e**). However, upregulation of Shal currents was 1.5-fold greater in dendrites than in the cell body (**Fig. 2e**).

Synthesis of Dα7 and Shal were differentially regulated

The increase in total Dα7 and Shal protein levels following prolonged synaptic blockade (**Figs. 1** and **2**), suggests the involvement of protein synthesis. To directly test this, and to examine whether regulation occurs at the transcriptional or translational level, we used actinomycin D to inhibit gene transcription, and either anisomycin or cycloheximide to block protein translation in mock- and curare-treated cultured brains (protocol 1, see Online Methods; **Fig. 3a,b**). As expected, the increases in Dα7 and Shal protein levels following curare treatment were both blocked by anisomycin and cycloheximide (**Fig. 3b** and **Supplementary Fig. 5a**), confirming that the synthesis of new protein is required in both cases. By contrast, actinomycin D blocked only the increase in Shal K^+ channels, and not Dα7 receptors (**Fig. 3a**), suggesting that Shal is transcriptionally regulated in this system.

To further test the differential regulation of Dα7 and Shal, we examined mEPSCs and I_A currents in identified motor neurons when either transcription or translation was inhibited. We used actinomycin D to block transcription and anisomycin to block translation. Synaptic blockade induced an increase in mEPSC and I_A amplitudes, as expected (**Fig. 3c**,**d**). When cultures were incubated with anisomycin, the increase in both mEPSC and I_A amplitudes were blocked (**Fig. 3c**,**d**), confirming again the involvement of protein synthesis. By contrast, inhibition of transcription by actinomycin D blocked only the upregulation of Shal K^+ currents, and not mEPSC amplitudes (**Fig. 3c**,**d**). Thus, immunoblot analyses and electrophysiological recordings both showed that synaptic inactivity induced an increase in translation of Dα7 receptors and an increase in transcription of *Shal*.

Given that the increase in Shal channels occured not during the 24 h of synaptic inhibition but during the 30-min period of recovery of synaptic transmission (see above; **Fig. 2**), we were surprised that regulation occurred at the transcriptional level. We further tested this finding by comparing *Shal* expression from the endogenous *Shal* gene to expression from an epitope (haemagglutinin (HA))-tagged *Shal* transgene (*UAS–HA-Shal*) lacking transcriptional regulatory domains. We generated a transgenic line in which *UAS–HA-Shal* expression was driven by *RRa-GAL4*. After 24 h of either mock or curare treatment (wash and recovery; protocol 1, see Online Methods), cultures were immunostained using anti-HA or anti-Shal. We found that synaptic blockade did not induce an increase in anti-HA signal but did induce a clear increase in anti-Shal signal in both somas and dendrites (**Fig. 3e** and **Supplementary Fig. 5b**,**c**). An increase in the amount of Shal protein expressed from the endogenous *Shal* gene, but not from an exogenous transgene, is consistent with regulation at the transcriptional level.

Increase in Shal was dependent on Dα7 nAChRs

We next examined the relationship between the increase in Dα7 receptors and the increase in Shal channels that both followed prolonged synaptic inactivity. The increase in Dα7 receptor levels occurred first, because it was evident immediately after curare treatment (**Fig. 2c**). By contrast, the increase in Shal channels and current required a subsequent 30–60-min recovery period of synaptic transmission (**Fig. 2**). These results suggest that the upregulation of Dα7 was triggered more 'directly' by synaptic inactivity and that upregulation of Shal channels occurred in response to this increase in Dα7 receptors. To test this possibility, we first examined whether Shal currents were upregulated in the absence of Dα7. We used *RRa-GAL4* to drive expression of *UAS–mCD8-GFP* in a Dα7-deficient mutant background ($D\alpha7^{P\Delta EY6}$; which is a null mutant for the gene encoding Dα7) and recorded mEPSCs and Shal K^+ currents from identified motor neurons before and after curare treatment (protocol 1, see Online Methods). In contrast to wild-type motor neurons, motor neurons lacking Dα7 did not exhibit an increase in Shal K+ currents following curare treatment (**Fig. 4a**). Notably, mEPSCs were increased with synaptic blockade (control: 8.71 ± 0.55 pA, $n = 12$; treated: 10.98 ± 0.72 pA, $n = 11$; **Fig. 4b**), although to a lesser extent than in wild-type neurons (**Fig. 1c**), suggesting that there was some redundancy or compensation by other nAChR subunits that was revealed or developed in the absence of Dα7.

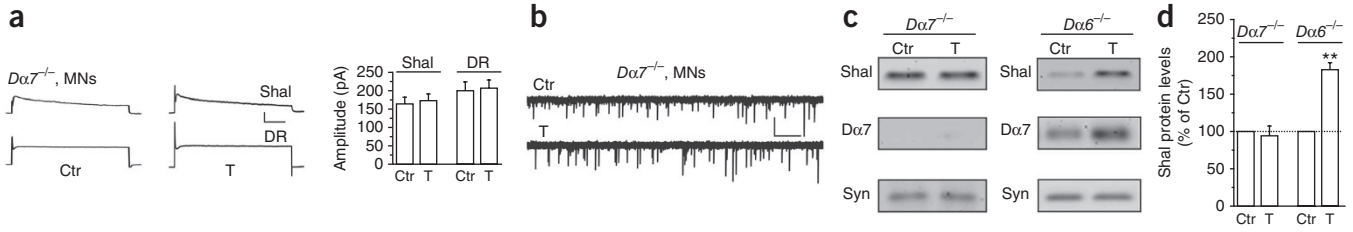

Figure 4 Dα7 receptors were essential for the increased expression of Shal channels. (**a**) Representative I_A (Shal-mediated) and delayed rectifier currents isolated from mock treated (control) and curare-treated (treated) *Dα7*$^{P\Delta EY}$ (*Dα7*$^{-/-}$) mutant motor neurons (left); treatment protocol 1 was used (see Online Methods). Quantitative analyses (right) showed no significant differences for Shal or delayed rectifier (DR) currents between control and treated cells. $n = 15$ (control) and 12 (treated). Scale bars: 100 pA, 25 ms. (**b**) Representative mEPSCs from control and treated *Dα7*$^{-/-}$ mutant motor neurons. Scale bars: 10 pA, 5 s. (**c**,**d**) Representative immunoblots (**c**) and quantitative analyses (**d**) of Shal and Dα7 protein levels in control and treated whole brains from *Dα7*$^{-/-}$ (left) and *nAcRα-30D*^{DAS2} (*Dα6*$^{-/-}$) (right) mutant flies. Syntaxin (Syn) was used as a loading control. Note that the Dα7 protein level was still increased in the curare-treated brains from *nAcRα-30D*^{DAS2} flies. $n = 4$ for each condition. Error bars: s.e.m. $^{**}P < 0.01$, Student's *t* test. Full-length blots and gels are shown in **Supplementary Figure 10**.

In addition, we compared Shal protein levels from wild-type and *Dα7*null mutant brains that were similarly mock or curare treated (wash and recovery). Immunoblot analyses showed no upregulation of Shal protein in the absence of Dα7 (**Fig. 4c**,**d**). As Dα7 subunits are among three nAChR subunits in *Drosophila* (Dα5 (encoded by *nAcRα-34E*), Dα6 (encoded by *nAcRα-30D*) and Dα7) that are ~60% identical to vertebrate α7 nAChR subunits[23], we also examined a null mutant for Dα6 (*nAcRα-30D*^{DAS2}). Prolonged inactivity followed by recovery of synaptic transmission resulted in increased Shal protein levels in the absence of Dα6 (**Fig. 4c**,**d**). Altogether, these results indicated that the increase in Shal K^+ channels following synaptic blockade had a specific requirement for Dα7 receptors.

Ca^{2+} was essential for the increase in Shal K^+ channels

If Shal channel expression was upregulated by an increase in Dα7 receptors, what was the signaling pathway from Dα7 to *Shal* transcription? We showed that both the increase in Dα7 and the recovery of synaptic transmission were key events in this pathway. As α7 receptors have been reported to have greater Ca^{2+} permeability than other nAChRs[18,19], we tested whether Ca^{2+} was an essential secondary messenger in this pathway. To do this, we used the Ca^{2+} chelator BAPTA in our intracellular recording solution. Cultures were mock or curare treated, antagonist was washed out for 3 min and then individual motor neurons were monitored by whole-cell recording for the next 20–30 min (protocol 3, see Online Methods), during which time Shal currents were actively upregulated. **Figure 5** shows scatter plots representing Shal K^+ current amplitudes at 25–30 min versus 5–10 min. Using normal intracellular solution in the pipet, synaptic blockade increased the ratio of I_A(25–30 min) / I_A(5–10 min) from 208 ± 17 pA to 378 ± 24 pA, as expected (**Fig. 5a**,**b** and **Supplementary Fig. 6**). To further confirm that Shal K^+ currents were indeed acutely upregulated, we used actinomycin D or anisomycin to block transcription or translation, respectively, and monitored Shal currents following antagonist washout. Indeed, ratios of I_A(25–30 min) / I_A(5–10 min) from single cells were no longer increased in the presence of these inhibitors (**Supplementary Fig. 6c**,**d**), demonstrating that the increase in Shal currents was a result of transcriptionally upregulated channels. We then monitored Shal currents after curare treatment with BAPTA included in our intracellular solution. We found that curare treatment no longer increased Shal K^+ currents, and I_A(25–30 min) / I_A(5–10 min) ratios were close to 1:1 (197 ± 11 pA / 205 ± 13 pA; **Fig. 5c**), as seen for untreated cells (**Fig. 5a**).

As nAChRs can also induce Ca^{2+} release from intracellular Ca^{2+} stores, we tested the contribution of Ca^{2+} from internal stores to triggering *Shal* expression. We monitored Shal K^+ currents in individual motor neurons during the ~25–30 min of recovery following synaptic blockade, but during this time we used thapsigargin to deplete intracellular Ca^{2+} stores. Inactivity-induced increases in I_A(25–30 min) / I_A(5–10 min) ratios were not blocked by thapsigargin (**Fig. 5d**). Together, our results suggested that the rise in intracellular Ca^{2+} (possibly mediated by new Dα7 receptors), and not intracellular Ca^{2+} stores, was required to trigger the increase in Shal channels.

CaMKII was essential for upregulation of Shal

Ca^{2+}/calmodulin-dependent kinases are well-known Ca^{2+} targets in a variety of synaptic plasticity and homeostatic pathways. We therefore

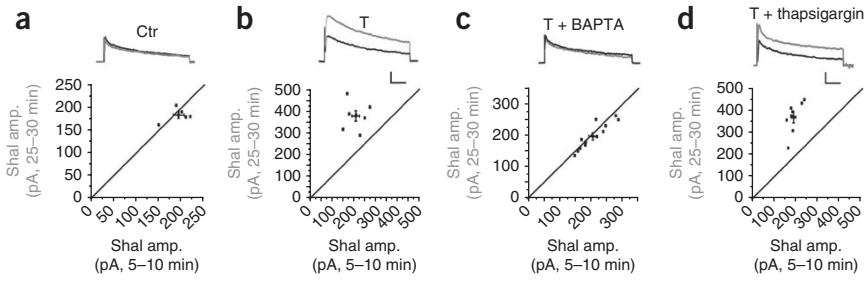

Figure 5 Ca^{2+} influx through Dα7 receptors was required for the increase in Shal channels. (**a**,**b**) Shal currents were recorded in motor neurons from mock-treated (control, **a**) or curare-treated (with 3 min washout of curare, protocol 3, Online Methods) (treated, **b**) cultures. Only the cells that were patched within 5–10 min after washout were used. Shal currents were continually monitored for the following 25–30 min. Representative Shal currents from control and treated cells are shown: one trace from 5–10 min after washout (black) and the other trace from the same cell at 25–30 min after washout (gray). Scatter plots of Shal amplitudes in individual cells at 5–10 min and 25–30 min are shown; means ± s.e.m. are also indicated. $n = 5$–6 for each condition. Scale bars: 100 pA, 25 ms. (**c**,**d**) Representative traces and scatter plots from treated cultures; the recording protocols were similar to those used for experiments in **a** and **b**. Recordings for **c** were performed in the conventional whole-cell mode with BAPTA included in the internal solution. Recordings for **d** were performed with thapsigargin pre-incubated in the external solution and present throughout recordings. $n = 8$–12 for each condition. Scale bars: 100 pA, 25 ms. See also **Supplementary Figure 6**.

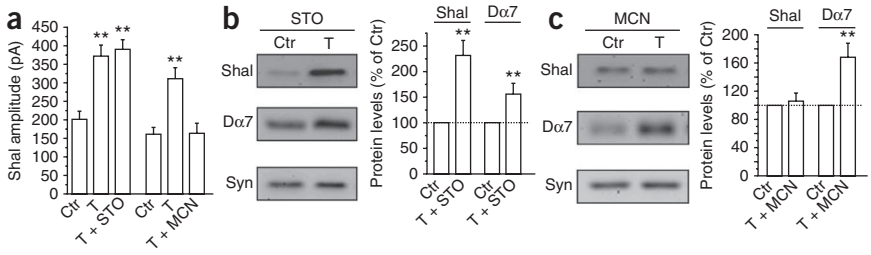

Figure 6 Activation of CaMKII, but not CaMKK, was required for the increase in Shal channel expression. (**a**) Quantitative analyses of Shal current amplitudes recorded from motor neurons in mock-treated (control) or curare-treated (treated) cultures; treatment protocol 1 (see Online Methods) was used, with STO-609 (STO) or Myr-CaMKIINtide (MCN) present only during the recovery period and recording. $n = 8–12$ for each condition. (**b**,**c**) Representative immunoblots (left) and quantitative analyses (right) of Shal and Dα7 protein levels in control and treated conditions, with STO or MCN present during washout only. Syntaxin (Syn) was used as a loading control. $n = 4$ for each condition. Error bars: s.e.m. $^{**}P < 0.01$, Student's t test. Full-length blots and gels are shown in **Supplementary Figure 10**.

investigated their potential role in signaling the upregulation of *Shal*. Cultures were mock and curare treated according to protocol 1 (see Online Methods). During the 30-min recovery period of synaptic transmission following antagonist washout, we used myristoylated CaMKII-Ntide (Myr-CaMKIINtide) and STO-609 to inhibit CaMKII and Ca2+/calmodulin-dependent protein kinase kinase (CaMKK) activity, respectively. Whereas synaptic blockade still increased Shal K^+ current amplitudes in the presence of STO-609, the increase in Shal currents was blocked in the presence of Myr-CaMKIINtide (**Fig. 6a**), suggesting that CaMKII was essential for the upregulation of Shal channels. These results were further confirmed in whole brains. Curare treatment induced an increase in Shal protein in the presence of STO-609, but this increase was completely blocked by Myr-CaMKIINtide (**Fig. 6b**,**c**). Thus, CaMKII was likely to be the target of the Ca^{2+} influx through the new Dα7 receptors, and a key component in the signaling pathway triggering upregulation of Shal channels.

We next tested whether activation of CaMKII was sufficient to upregulate Shal K^+ currents. To do this, we used the *UAS-CaMKII*^{T287D} transgene, which encodes a constitutively active form of CaMKII ($CaMKII^{T287D}$)[24]. We used *RRa-GAL4* to drive expression of *UAS–mCD8-EGFP* and *UAS-CaMKII*^{T287D} in motor neurons. We found that Shal currents were indeed increased, nearly twofold, in these motor neurons compared to the currents in wild-type motor neurons (**Supplementary Fig. 7**), suggesting that active CaMKII alone up–regulated Shal channels.

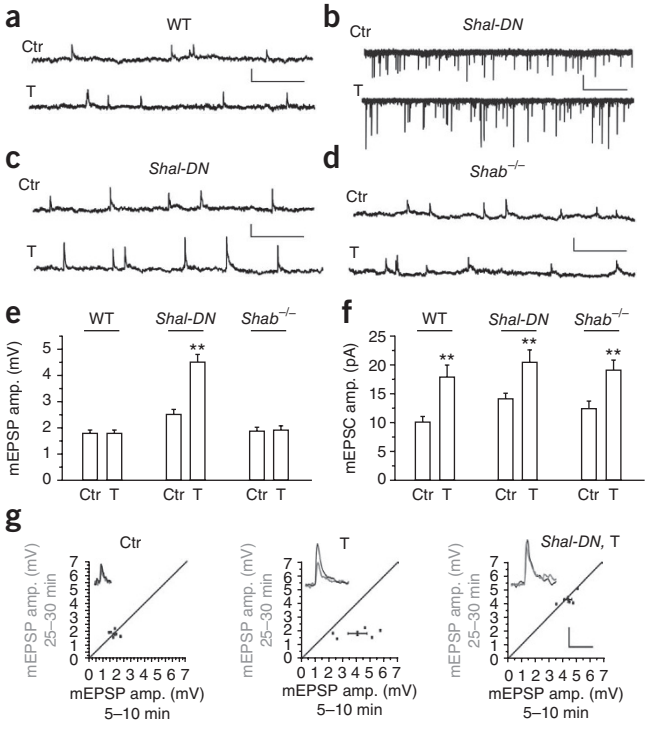

Figure 7 Higher number of Shal channels stabilized synaptic potentials. (**a**,**c**,**d**) Representative mEPSPs recorded from wild-type motor neurons (**a**, WT), motor neurons expressing a dominant-negative Shal subunit (**c**, DNKv4, Shal-DN) and *Shab*^{3} motor neurons (**d**, *Shab*$^{-/-}$). Motor neurons were either mock treated (control) or curare treated (treated) (using protocol 1, see Online Methods). Scale bars: 2 mV, 1 s. (**b**) mEPSCs from control and treated DNKv4 motor neurons. Scale bars: 10 pA, 5 s. (**e**) mEPSP amplitudes for wild-type ($n = 12–14$), DNKv4 ($n = 9–11$) and *Shab*$^{-/-}$ ($n = 9–11$) control and treated motor neurons. (**f**) mEPSC amplitudes from the same conditions as those shown in **b**, from wild-type ($n = 12$), DNKv4 ($n = 9–13$) and *Shab*$^{-/-}$ ($n = 12$) control and treated motor neurons. (**g**) mEPSPs from control (left) and treated (middle) wild-type motor neurons, or treated motor neurons expressing DNKv4 (right). Cells were monitored after 3 min of antagonist washout (protocol 3, see Online Methods). Shown are mEPSPs recorded at 5–10 min after washout (black, inset) and then at 25–30 min after washout (gray, inset). Scatter plots show mEPSP amplitudes from individual cells at 5–10 min and 25–30 min after washout; means are also indicated. $n = 5$ for each condition. Scale bars: 2 mV, 0.1 s. Error bars: s.e.m. $^{**}P < 0.01$, Student's t test. See also **Supplementary Table 1**.

The increase in Shal stabilized synaptic potentials

Why does the homeostatic upregulation of Dα7 receptors trigger an increase in a hyperpolarizing current? Most reported cell-intrinsic changes to synaptic inactivity increase excitability, thereby contributing to the homeostatic response. An increase in Shal K^+ currents, however, would most probably decrease excitability. One possibility is that the increase in Shal K^+ channels serves as a mechanism to regulate the homeostatic response, keeping potentiation 'in check' and preventing overexcitation. To investigate this possibility, we examined the effects of the increase in Shal K^+ currents on synaptic potentials (using treatment protocol 1, see Online Methods). Notably, we found that amplitudes of mEPSCs were significantly larger following curare treatment ($P < 0.01$; **Fig. 7**), but miniature excitatory postsynaptic potentials (mEPSPs) were stable (control, 1.78 ± 0.12 mV; treated, 1.80 ± 0.14 mV; **Fig. 7a**,**e**). This was not due to a difference in resting membrane potential, as control and curare-treated neurons had similar passive membrane properties (**Supplementary Table 1**).

To test this hypothesis more directly, we recorded from motor neurons expressing a dominant-negative Shal subunit (DNKv4) that completely blocks Shal K^+ channel function[15]. In the absence of Shal K^+ channel function, mEPSCs were increased after curare treatment (**Fig. 7**), similarly to in wild-type motor neurons. Thus, homeostatic upregulation of Dα7 receptors occurs independently of Shal K^+ channel function. We next examined mEPSPs from control and curare-treated DNKv4 motor neurons. Synaptic potentials were not

stabilized as they were in wild-type motor neurons. mEPSP amplitudies were significantly larger after synaptic inhibition in the absence of Shal function (control, 2.5 ± 0.21 mV; treated, 4.51 ± 0.30 mV; $P < 0.01$ **Fig. 7**), indicating that Shal channels were indeed required for stabilizing synaptic potentials. To test whether this function was specific to Shal channels, we performed the same experiments using a *Shab*-null mutant (*Shab*[3]). Although loss of Shab removed nearly all of the delayed rectifier K^+ current present in these neurons[11], mEPSPs remained stabilized after curare treatment (**Fig. 7**).

Finally, we monitored mEPSPs in single neurons during the 30 min following antagonist washout (protocol 3, see Online Methods). mEPSPs from curare-treated neurons were increased at 5–10 min, presumably owing to the increase in Dα7 receptors, then stabilized to control amplitudes 25–30 min after antagonist washout (**Fig. 7g**). To confirm that the acute mEPSP upregulation at 5–10 min followed by stabilization at 25–30 min was regulated by translation of Dα7-encoding mRNA and transcription of *Shal*, we repeated these experiments using actinomycin D or anisomycin to block transcription or translation, respectively. When transcription was blocked, mEPSP amplitudes were greater than those of untreated cells but were not stabilized after 25–30 min (**Supplementary Fig. 8a**). When translation was inhibited, the initial increase in mEPSP amplitude (at 5–10 min) was unchanged compared to untreated cells and remained constant during the 30 min of monitoring (**Supplementary Fig. 8b**). Altogether, these results suggested that following curare treatment Dα7 receptors were translationally upregulated, resulting in larger mEPSPs, and then Shal was transcriptionally upregulated, resulting in the stabilization of mEPSPs. When the mEPSPs were monitored in motor neurons expressing DNKv4, increased mEPSP amplitudes were no longer stabilized (**Fig. 7g**). Together, our studies showed that the increase in Dα7 receptors following synaptic inactivity triggered an increase in Shal K^+ channels that served to stabilize synaptic potentials.

DISCUSSION

Synaptic homeostatic mechanisms serve to stabilize neural circuits in response to changes in activity. Studies of synaptic homeostasis in *Drosophila* have largely focused on the NMJ and underlying presynaptic mechanisms[2]. Reports of homeostatic changes at interneuronal synapses in *Drosophila* have mostly been limited to structural changes[25–27]. In this study, we showed that inhibition of nAChRs resulted in mEPSCs that were increased in amplitude and frequency, indicating that there were both pre- and postsynaptic effects. Focusing on postsynaptic changes, we found that the number of Dα7 receptors was preferentially increased, mediating mEPSCs with larger amplitudes, faster decay rates and, probably, increased Ca^{2+} influx. However, this homeostatic response did not require the Dα7 receptor, as mEPSCs were increased in the Dα7-deficient mutant, suggesting that one or more other nAChRs are upregulated in the absence of the Dα7 receptor. Thus, excitatory neurons exhibit a resilient homeostatic increase in nAChRs to compensate for conditions of inactivity. It is interesting to note the lack of this same plasticity in lateral cluster even-skipped-expressing interneurons. As interneurons are generally thought to be inhibitory (see ref. 28), this would also contribute to the homeostatic response. Our results parallel the widely observed homeostatic increase in GluA1- or GluA2-containing receptors that is restricted to excitatory mammalian neurons[1,3].

Activity-dependent plasticity of muscular nAChRs during development of the vertebrate NMJ has long been studied[29]. Perhaps more relevant to our findings, however, is the increase in neuronal nAChRs that occurs following prolonged nicotine exposure[18]. Studies have suggested that desensitization of the receptors to nicotine triggers a homeostatic response that upregulates nAChRs[8]. In our study, direct antagonist exposure resulted in an increase in the Dα7 nAChR. The Dα7 receptor of *Drosophila* is highly homologous to the vertebrate α7-nAChR subunit, with ~60% amino acid identity. In the mammalian CNS, the homomeric α7 receptor is one of the most abundant and widely expressed classes of nAChRs[19], and homeostatic upregulation of α7 has been speculated to contribute to the progression of Alzheimer's disease[30]. Thus, *Drosophila* central neurons may provide a useful model for studying neuronal nAChR-mediated homeostasis mechanisms that contribute to pathological conditions such as nicotine addiction and Alzheimer's disease.

We showed that the inactivity-induced increase in the Dα7 nAChR was followed by an increase in the voltage-dependent Shal K^+ channel. Shal K^+ channels are highly conserved and underlie the somatodendritic A-type K^+ current in most neurons[31]. Shal currents have been shown to modulate dendritic excitability, by regulating backpropagating action potentials and postsynaptic potentials[32–34]. Our data suggest that inactivity induces an increase in the number of Dα7 receptors, mediated by enhanced translation of the encoding mRNA, that in turn results in larger mEPSCs. Although the homeostatic increase in mEPSCs was not dependent on the Dα7 receptor, we showed that the upregulation of Shal channels required Dα7. Dα7 receptors probably carry a substantial influx of Ca^{2+} than other nAChRs, which in turn activates CaMKII, leading to rapid (<30 min) upregulation of Shal channels. As CaMKII has previously been implicated in receptor homeostasis and Shal channel regulation[35–37], the localization and regulation of CaMKII is likely to be critical to its roles in these different pathways.

What is the function of this upregulation of Shal K^+ channels that is observed after synaptic blockade and an increase in Dα7 receptors? Previously, cell-intrinsic changes have mostly been suggested to increase excitability and contribute to homeostasis[1,4–6,38]. However, the upregulation of Shal K^+ current is intriguing because it is likely to counter homeostatic mechanisms. mEPSPs recorded in cell bodies are likely to represent larger mEPSPs in dendrites[39] that would activate local Shal channels, which in turn would modulate PSPs. EPSPs, both large and small, have been shown to activate Shal K^+ channels in mammalian neurons, similarly reducing EPSPs[34,40]. Indeed, we found that the increase in Shal current stabilized synaptic potentials that would otherwise be increased by homeostatic pathways. Modulation of synaptic currents to match a fixed, or stable, synaptic potential has been proposed to underlie a homeostatic solution to the difference in dendritic arbor sizes and input resistances of *Drosophila* projection neurons[41]. A more generalized function may be to boost activity by increasing nAChRs when activity is lowered or blocked and then, when circuits run the risk of becoming overactive, to upregulate Shal K^+ channels to temper synaptic potentials. This represents a previously unknown mechanism for fine-tuning the homeostatic response and preventing overexcitation.

The increase in transcription of Shal channel-encoding genes in response to increased translation of Dα7-encoding mRNA brings up many intriguing questions. For example, why is the up- and down-regulation of activity controlled at two different loci? That is, why not simply up- and downregulate Dα7 as required for activity? As upregulation of Dα7 is slow (for example, it requires 24 h of synaptic blockade to upregulate nAChRs), one possibility is that it is not beneficial for the cell to down-regulate the receptors, given that replacement and a return to normal activity would probably be very slow. Rapid upregulation of Shal channels has perhaps evolved to be a better solution. It will also be important to understand whether there

is any specificity, or co-ordination with sites of activity or inactivity, for the trafficking and subcellular localization of Shal K^+ channels.

METHODS

Methods and any associated references are available in the online version of the paper at http://www.nature.com/natureneuroscience/.

Note: Supplementary information is available on the Nature Neuroscience website.

ACKNOWLEDGMENTS

We thank G. Waro for genetic crosses and technical assistance. We thank H. Bellen (Baylor College of Medicine) for the antibody to Dα7 and the Dα7-deficient mutant line, S. Sigrist (Institute for Biology/Genetics) for the *UAS–nAcRα-18C-EGFP* fly line, M. Fujioka (Thomas Jefferson University) for the *RRa-GAL4*, *RN2-GAL4* and *EL-GAL4* fly lines, S. Singh (State University of New York, Buffalo) for the *Shab[3]* line, and E. Gundelfinger and U. Thomas (Leibniz Institute for Neurobiology) for the antibodies to *Drosophila* nAChRs. We also thank C. Yeung for carrying out genetic mapping and crosses for the transgenic *HA-Shal* line. S.T. is supported by a grant from the US National Institutes of Health (R01 GM083335).

AUTHOR CONTRIBUTIONS

Y.P. conducted all of the experiments and analyzed all of the data. S.T. supervised the project and wrote the majority of the manuscript.

COMPETING FINANCIAL INTERESTS

The authors declare no competing financial interests.

Published online at http://www.nature.com/natureneuroscience/.
Reprints and permissions information is available online at http://www.nature.com/reprints/index.html.

1. Turrigiano, G. Too many cooks? Intrinsic and synaptic homeostatic mechanisms in cortical circuit refinement. *Annu. Rev. Neurosci.* **34**, 89–103 (2011).
2. Davis, G.W. Homeostatic control of neural activity: from phenomenology to molecular design. *Annu. Rev. Neurosci.* **29**, 307–323 (2006).
3. Pozo, K. & Goda, Y. Unraveling mechanisms of homeostatic synaptic plasticity. *Neuron* **66**, 337–351 (2010).
4. Desai, N.S., Rutherford, L.C. & Turrigiano, G.G. Plasticity in the intrinsic excitability of cortical pyramidal neurons. *Nat. Neurosci.* **2**, 515–520 (1999).
5. Kuba, H., Oichi, Y. & Ohmori, H. Presynaptic activity regulates Na^+ channel distribution at the axon initial segment. *Nature* **465**, 1075–1078 (2010).
6. Baines, R.A., Uhler, J.P., Thompson, A., Sweeney, S.T. & Bate, M. Altered electrical properties in *Drosophila* neurons developing without synaptic transmission. *J. Neurosci.* **21**, 1523–1531 (2001).
7. Nataraj, K., Le Roux, N., Nahmani, M., Lefort, S. & Turrigiano, G. Visual deprivation suppresses L5 pyramidal neuron excitability by preventing the induction of intrinsic plasticity. *Neuron* **68**, 750–762 (2010).
8. De Biasi, M. & Dani, J.A. Reward, addiction, withdrawal to nicotine. *Annu. Rev. Neurosci.* **34**, 105–130 (2011).
9. Picciotto, M.R., Addy, N.A., Mineur, Y.S. & Brunzell, D.H. It is not "either/or": activation and desensitization of nicotinic acetylcholine receptors both contribute to behaviors related to nicotine addiction and mood. *Prog. Neurobiol.* **84**, 329–342 (2008).
10. Fenster, C.P., Whitworth, T.L., Sheffield, E.B., Quick, M.W. & Lester, R.A. Upregulation of surface α4β2 nicotinic receptors is initiated by receptor desensitization after chronic exposure to nicotine. *J. Neurosci.* **19**, 4804–4814 (1999).
11. Tsunoda, S. & Salkoff, L. The major delayed rectifier in both *Drosophila* neurons and muscle is encoded by Shab. *J. Neurosci.* **15**, 5209–5221 (1995b).
12. Tsunoda, S. & Salkoff, L. Genetic analysis of *Drosophila* neurons: Shal, Shaw, and Shab encode most embryonic potassium currents. *J. Neurosci.* **15**, 1741–1754 (1995a).
13. Lee, D. & O'Dowd, D.K. Fast excitatory synaptic transmission mediated by nicotinic acetylcholine receptors in *Drosophila* neurons. *J. Neurosci.* **19**, 5311–5321 (1999).
14. Leung, H.T., Branton, W.D., Phillips, H.S., Jan, L. & Byerly, L. Spider toxins selectively block calcium currents in *Drosophila*. *Neuron* **3**, 767–772 (1989).
15. Ping, Y. *et al.* Shal/K_v4 channels are required for maintaining excitability during repetitive firing and normal locomotion in *Drosophila*. *PLoS ONE* **6**, e16043 (2011).
16. Su, H. & O'Dowd, D.K. Fast synaptic currents in *Drosophila* mushroom body Kenyon cells are mediated by α-bungarotoxin-sensitive nicotinic acetylcholine receptors and picrotoxin-sensitive GABA receptors. *J. Neurosci.* **23**, 9246–9253 (2003).
17. Schmidt, H. *et al.* The embryonic central nervous system lineages of *Drosophila melanogaster*. II. Neuroblast lineages derived from the dorsal part of the neuroectoderm. *Dev. Biol.* **189**, 186–204 (1997).
18. Gotti, C. *et al.* Structural and functional diversity of native brain neuronal nicotinic receptors. *Biochem. Pharmacol.* **78**, 703–711 (2009).
19. Albuquerque, E.X., Pereira, E.F., Alkondon, M. & Rogers, S.W. Mammalian nicotinic acetylcholine receptors: from structure to function. *Physiol. Rev.* **89**, 73–120 (2009).
20. Aracava, Y., Pereira, E.F., Maelicke, A. & Albuquerque, E.X. Memantine blocks α7* nicotinic acetylcholine receptors more potently than *N*-methyl-D-aspartate receptors in rat hippocampal neurons. *J. Pharmacol. Exp. Ther.* **312**, 1195–1205 (2005).
21. Brickley, S.G., Revilla, V., Cull–Candy, S.G., Wisden, W. & Farrant, M. Adaptive regulation of neuronal excitability by a voltage-independent potassium conductance. *Nature* **409**, 88–92 (2001).
22. Pulver, S.R. & Griffith, L.C. Spike integration and cellular memory in a rhythmic network from Na+/K+ pump current dynamics. *Nat. Neurosci.* **13**, 53–59 (2010).
23. Grauso, M., Reenan, R.A., Culetto, E. & Sattelle, D.B. Novel putative nicotinic acetylcholine receptor subunit genes, *Dα5*, *Dα6* and *Dα7*, in *Drosophila melanogaster* identify a new and highly conserved target of adenosine deaminase acting on RNA-mediated A-to-I pre-mRNA editing. *Genetics* **160**, 1519–1533 (2002).
24. Griffith, L.C. *et al.* Inhibition of calcium/calmodulin-dependent protein kinase in *Drosophila* disrupts behavioral plasticity. *Neuron* **10**, 501–509 (1993).
25. Tripodi, M., Evers, J.F., Mauss, A., Bate, M. & Landgraf, M. Structural homeostasis: compensatory adjustments of dendritic arbor geometry in response to variations of synaptic input. *PLoS Biol.* **6**, e260 (2008).
26. Kremer, M.C. *et al.* Structural long-term changes at mushroom body input synapses. *Curr. Biol.* **20**, 1938–1944 (2010).
27. Bushey, D., Tononi, G. & Cirelli, C. Sleep and synaptic homeostasis: structural evidence in *Drosophila*. *Science* **332**, 1576–1581 (2011).
28. Chou, Y.H. *et al.* Diversity and wiring variability of olfactory local interneurons in the *Drosophila* antennal lobe. *Nat. Neurosci.* **13**, 439–449 (2010).
29. Lichtman, J.W. & Colman, H. Synapse elimination and indelible memory. *Neuron* **25**, 269–278 (2000).
30. Small, D.H. Network dysfunction in Alzheimer's disease: does synaptic scaling drive disease progression? *Trends Mol. Med.* **14**, 103–108 (2008).
31. Jerng, H.H., Pfaffinger, P.J. & Covarrubias, M. Molecular physiology and modulation of somatodendritic A-type potassium channels. *Mol. Cell. Neurosci.* **27**, 343–369 (2004).
32. Chen, X. *et al.* Deletion of *Kv4.2* gene eliminates dendritic A-type K^+ current and enhances induction of long-term potentiation in hippocampal CA1 pyramidal neurons. *J. Neurosci.* **26**, 12143–12151 (2006).
33. Kim, J., Jung, S.C., Clemens, A.M., Petralia, R.S. & Hoffman, D.A. Regulation of dendritic excitability by activity-dependent trafficking of the A-type K^+ channel subunit Kv4.2 in hippocampal neurons. *Neuron* **54**, 933–947 (2007).
34. Cai, X. *et al.* Unique roles of SK and Kv4.2 potassium channels in dendritic integration. *Neuron* **44**, 351–364 (2004).
35. Thiagarajan, T.C., Piedras–Renteria, E.S. & Tsien, R.W. α- and β-CaMKII. Inverse regulation by neuronal activity and opposing effects on synaptic strength. *Neuron* **36**, 1103–1114 (2002).
36. Groth, R.D., Lindskog, M., Thiagarajan, T.C., Li, L. & Tsien, R.W. β Ca^{2+}/CaM-dependent kinase type II triggers upregulation of GluA1 to coordinate adaptation to synaptic inactivity in hippocampal neurons. *Proc. Natl. Acad. Sci. USA* **108**, 828–833 (2011).
37. Varga, A.W. *et al.* Calcium–calmodulin-dependent kinase II modulates Kv4.2 channel expression and upregulates neuronal A-type potassium currents. *J. Neurosci.* **24**, 3643–3654 (2004).
38. Misonou, H. Homeostatic regulation of neuronal excitability by K^+ channels in normal and diseased brains. *Neuroscientist* **16**, 51–64 (2010).
39. Magee, J.C. & Cook, E.P. Somatic EPSP amplitude is independent of synapse location in hippocampal pyramidal neurons. *Nat. Neurosci.* **3**, 895–903 (2000).
40. Hoffman, D.A., Magee, J.C., Colbert, C.M. & Johnston, D. K^+ channel regulation of signal propagation in dendrites of hippocampal pyramidal neurons. *Nature* **387**, 869–875 (1997).
41. Kazama, H. & Wilson, R.I. Homeostatic matching and nonlinear amplification at identified central synapses. *Neuron* **58**, 401–413 (2008).

ONLINE METHODS

Fly stocks. We used w^{1118} as wild-type flies in this study. *RRa-GAL4, RN2-GAL4* and *EL-GAL4* lines were provided by M. Fujioka[42], the $D\alpha7^{P\Delta EY6}$ (ref. 43) line was provided by H. Bellen, the $nAcR\alpha\text{-}30D^{DAS2}$ (ref. 44) and *UAS-CaMKII*^{T287D} (ref. 24) lines were obtained from the Bloomington *Drosophila* stock center, and the $Shab^{3}$ (ref. 45) line was provided by S. Singh. We generated the transgenic line expressing the dominant-negative Shal subunit (*UAS-DNKv4*). In brief, the *Shal2* cDNA was modified to encode an HA tag (YPYDVPDYA) fused to the N terminus and to have a W362F substitution; this transgenic line and its function were previously described[15]. For the *UAS–HA-Shal* transgenic line, we modified the *Shal2* cDNA to include two tandem HA tags in an extracellular loop of the channel (after Cys221), then subcloned this cDNA into the *pUAST* transformation vector. This construct was generated by GenScript, Inc. Microinjection of the *pUAST–HA-Shal2* construct into embryos was performed by Rainbow Transgenic Flies. We screened, mapped and balanced transgenic lines into stable stocks by standard procedures.

Whole-brain and neuronal cultures. For whole-brain cultures, we anaesthetized adult flies (<2 days after eclosion), then submerged them in ice-cold Schneider's *Drosophila* medium on a clean glass slide. We dissected brains quickly and carefully with retinas left intact; damaged brains were discarded. We placed 5–6 brains in a 50 µl drop of culture medium (18% FBS (vol/vol), 100 units ml^{-1} penicillin, 100 µg ml^{-1} streptomysin in Schneider's *Drosophila* medium) on a glass coverslip. We incubated cultures in a humidified chamber at 21–23 °C and refreshed the culture medium every 12 h.

For embryonic neuronal cultures, we dissociated embryos aged 5–6 h (at 25 °C, stage 9–10) into culture medium, as previously described[11,12]. Note that for curare-treated whole-brain cultures, we washed for 1 h following treatment, whereas embryonic neuronal cultures were washed for 30 min. In order to monitor Shal currents or mEPSPs during the washout, we washed cultures for 3 min before recording in external solution.

We subjected cultured neurons and brains to three different treatment protocols, as described here. For protocol 1, we treated cultures with 30 µM tubocurare (curare) in culture medium, then washed antagonist out with fresh medium for ~3 min and incubated cultures in fresh medium for a recovery period of 30 min for electrophysiological recordings and 60 min for cultured brains. This was followed by recording (in appropriate recording solution), or immunoblot or immunostaining analysis. For protocol 2, we treated cultures with 30 µM curare in culture medium, and we then replaced the medium with recording solution for recording (with antagonist still present) or made samples for immunoblot analysis. For protocol 3, we treated cultures with 30 µM curare in culture medium and then washed out the antagonist with fresh medium for ~3 min, followed by recording (in appropriate recording solution). All curare treatments were for 24 h, unless otherwise specified.

Electrophysiology. We performed all recordings in the perforated-patch (400 µg ml^{-1} amphotericin B in the pipette), conventional whole-cell or cell-attached configuration, as indicated. We took recordings from GFP-labeled neurons from cultures 7 days after dissociation (7 d). To chronically suppress neuronal activity, we incubated cultures with 30 µM curare in culture medium at 6 d or 7 d for indicated times (15 min, 12 h and 24 h). We exchanged culture medium for external solution: 140 mM NaCl, 2 mM KCl, 6 mM $MgCl_2$, 0.5 mM $CaCl_2$, 5 mM HEPES, pH 7.2. We added tetrodotoxin (TTX) (1 µM) and picrotoxin (10 µM) to the external solution when recording mEPSCs and mEPSPs. We used choline-Cl instead of NaCl when recording Shal currents, with the exception of the Shal recordings shown in **Figure 5**. For the experiment shown in **Figure 5**, we added TTX (1 µM) and nifedipine (10 µM) to the external solution to block Na^{2+} and Ca^{2+} currents. We filled electrodes with internal solution (120 mM K-gluconate, 20 mM KCl, 10 mM HEPES, 1.1 mM ethylene glycol tetraacetic acid (EGTA), 2 mM $MgCl_2$, 0.1 mM $CaCl_2$, pH 7.2) for the mEPSP, mEPSC and firing pattern recordings shown in **Figure 7** and **Supplementary Figure 8**, and for all Shal current recordings. For the Shal current recordings shown in **Figure 5**, we included BAPTA (10 mM) in the internal solution, which was accommodated by decreasing K-gluconate to 110 mM. In some cases, we used CsCl instead of K-gluconate and KCl when recording mEPSCs. For cell-attached recordings, we filled pipettes with 140 mM NaCl, 6 mM $MgCl_2$, 0.5 mM $CaCl_2$, 5 mM HEPES, 0.001 mM TTX, 10 µM nifedipine (pH 7.2). Some cell-attached patches contained little to no current, most probably because axons can be easily mistaken for dendrites in these neurons; thus, we did not include currents <5 pA in amplitude. We performed all recordings at 22–24 °C. Electrode resistances for all perforated-patch and whole-cell recordings were 3–8 MΩ; gigaohm seals were obtained in all cases. For cell-attached recordings, electrode resistances were 7–9 MΩ, with >5 GΩ seals; tips were fire polished and inspected for uniform diameter.

We isolated Shal currents with a prepulse protocol, as previously described[15,46]. Briefly, we obtained total whole-cell K^+ currents using a voltage jump to +50 mV following a 500 ms prepulse of –125 mV. We used a 500 ms prepulse of –45 mV to completely inactivate Shal currents; the delayed rectifier current activated by a jump to +50 mV was then subtracted from the total K^+ current to obtain the Shal current. We recorded mEPSCs at –70 mV. In current-clamp experiments, we clamped the membrane current at 0 pA, and leaky cells (with resting membrane potentials above –55 mV) were discarded.

Statistical analyses. For mEPSCs and mEPSPs, we analyzed more than 50 events from each cell using Clampfit (Axon Instruments). We used 2 min recordings from each cell to ensure that each cell was equally represented in our analyses. mEPSC and mEPSP events were detected with detection thresholds of ~2 pA and ~0.4 mV, respectively. We fit the mEPSC deactivation kinetics with a standard double exponential function: $f(t) = A_1 e^{-t/\tau(\text{fast})} + A_2 e^{-t/\tau(\text{slow})} + C$. τ(fast) and τ(slow) are the time constants for the fast and slow components, and A_1 and A_2 are the amplitudes of the fast and slow components, respectively. We generated all data from at least three independent experiments, and data are shown as means with s.e.m. values. Statistical differences were determined using the Student's *t* test or Kolmogorov-Smirnov test.

Immunohistochemical and immunoblot analyses. We blindly separated sister cultures into two groups for mock and curare treatment on day 6. After 24 h, we rinsed cultures with PBS, fixed them with 4% formaldehyde (vol/vol) in PBS for 7–10 min, blocked (1% BSA or 5% goat serum, 0.1% sapponin in PBS, wt/vol) for 30–60 min, then incubated cultures with primary antibody overnight at 4 °C. Antibodies to the following proteins were used at the indicated concentrations: Dα7 (1:200)[43], Shal (1:100)[46], Syntaxin (1:200; Developmental Hybridoma Studies Bank (DHSB)), HA (1:200; Covance Research Products). After four washes (0.1% sapponin in PBS, 5 min each), we incubated cultures with fluorophore-conjugated secondary antibody (1:500; Jackson ImmunoResearch Laboratories) at 21–23 °C for 1 h, washed them again, then mounted them in *p*-phenylenediamine in 90% glycerol (vol/vol). We imaged control and treated cultures with a ×100 oil-immersion objective under the same conditions (for example, exposure times) for comparison. For anti-HA or anti-Shal immunostaining, we determined average gray values from somas after substracting background gray values using the Photoshop CS2 software.

For immunoblot analyses, we used primary antibodies tothe following proteins at the indicated concentrations, overnight at 21–23 °C: Dα1 (polyclonal antibody R14, 1:500)[47], Dα2 (monoclonal antibody 4F6, 1:200)[48], Dα7 (1:200)[43], Dβ1 (monoclonal antibody 3d2, 1:100)[49], Dβ2 (polyclonal antibody 4596, 1:500)[50], Shal (1:100)[46] and Syntaxin (1:100; DHSB).

42. Fujioka, M. *et al.* Even-skipped, acting as a repressor, regulates axonal projections in *Drosophila*. *Development* **130**, 5385–5400 (2003).
43. Fayyazuddin, A., Zaheer, M.A., Hiesinger, P.R. & Bellen, H.J. The nicotinic acetylcholine receptor Dα7 is required for an escape behavior in *Drosophila*. *PLoS Biol.* **4**, e63 (2006).
44. Watson, G.B. *et al.* A spinosyn–sensitive *Drosophila melanogaster* nicotinic acetylcholine receptor identified through chemically induced target site resistance, resistance gene identification, and heterologous expression. *Insect Biochem. Mol. Biol.* **40**, 376–384 (2010).
45. Hegde, P., Gu, G.G., Chen, D., Free, S.J. & Singh, S. Mutational analysis of the Shab-encoded delayed rectifier K(+) channels in *Drosophila*. *J. Biol. Chem.* **274**, 22109–22113 (1999).
46. Diao, F., Waro, G. & Tsunoda, S. Fast inactivation of Shal (K_v4) K^+ channels is regulated by the novel interactor SKIP3 in *Drosophila* neurons. *Mol. Cell. Neurosci.* **42**, 33–44 (2009).
47. Schulz, R. *et al.* Neuronal nicotinic acetylcholine receptors from *Drosophila*: two different types of alpha subunits coassemble within the same receptor complex. *J. Neurochem.* **74**, 2537–2546 (2000).
48. Jonas, P.E., Phannavong, B., Schuster, R., Schroder, C. & Gundelfinger, E.D. Expression of the ligand-binding nicotinic acetylcholine receptor subunit Dα2 in the *Drosophila* central nervous system. *J. Neurobiol.* **25**, 1494–1508 (1994).
49. Chamaon, K., Schulz, R., Smalla, K.H., Seidel, B. & Gundelfinger, E.D. Neuronal nicotinic acetylcholine receptors of *Drosophila melanogaster*: the α-subunit Dα3 and the β-type subunit ARD co–assemble within the same receptor complex. *FEBS Lett.* **482**, 189–192 (2000).
50. Chamaon, K., Smalla, K.H., Thomas, U. & Gundelfinger, E.D. Nicotinic acetylcholine receptors of *Drosophila*: three subunits encoded by genomically linked genes can co–assemble into the same receptor complex. *J. Neurochem.* **80**, 149–157 (2002).

doi:10.1038/nn.2969